

Improving photosensitivity without changing thermal reactivity in photochromic diarylbenzenes based on accurate prediction by DFT calculations

メタデータ	言語: English 出版者: Royal Society of Chemistry 公開日: 2021-06-03 キーワード (Ja): キーワード (En): 作成者: 北川, 大地, 高橋, 直子, 中濱, 龍源, 小畠, 誠也 メールアドレス: 所属: Osaka City University, Osaka City University, Osaka City University, Osaka City University
URL	https://ocu-omu.repo.nii.ac.jp/records/2020359

Improving photosensitivity without changing thermal reactivity in photochromic diarylbenzenes based on accurate prediction by DFT calculations

Daichi Kitagawa, Naoko Takahashi, Tatsumoto Nakahama, Seiya Kobatake

Citation	Photochemical & Photobiological Sciences. 19(5); 644-653.
Issue Date	2020-05-01
Type	Journal Article
Textversion	Author
Supplementary files	Supplementary information is available at https://doi.org/10.1039/D0PP00024H
Rights	The following article has been accepted by Photochemical & Photobiological Sciences. This is accepted manuscript version. The final, published version is available at https://doi.org/10.1039/D0PP00024H .
DOI	10.1039/D0PP00024H

Self-Archiving by Author(s)
Placed on: Osaka City University Repository

Daichi Kitagawa, Naoko Takahashi, Tatsumoto Nakahama, Seiya Kobatake. (2020). Improving photosensitivity without changing thermal reactivity in photochromic diarylbenzenes based on accurate prediction by DFT calculations. *Photochemical & Photobiological Sciences*. 19, 644-653. DOI: 10.1039/D0PP00024H

Improving Photosensitivity without Changing Thermal Reactivity in Photochromic Diarylbenzenes Based on Accurate Prediction by DFT Calculations

*Daichi Kitagawa**, *Naoko Takahashi*, *Tatsumoto Nakahama*, and *Seiya Kobatake**

Department of Applied Chemistry, Graduate School of Engineering, Osaka City University, 3-3-138 Sugimoto, Sumiyoshi-ku, Osaka 558-8585, Japan.

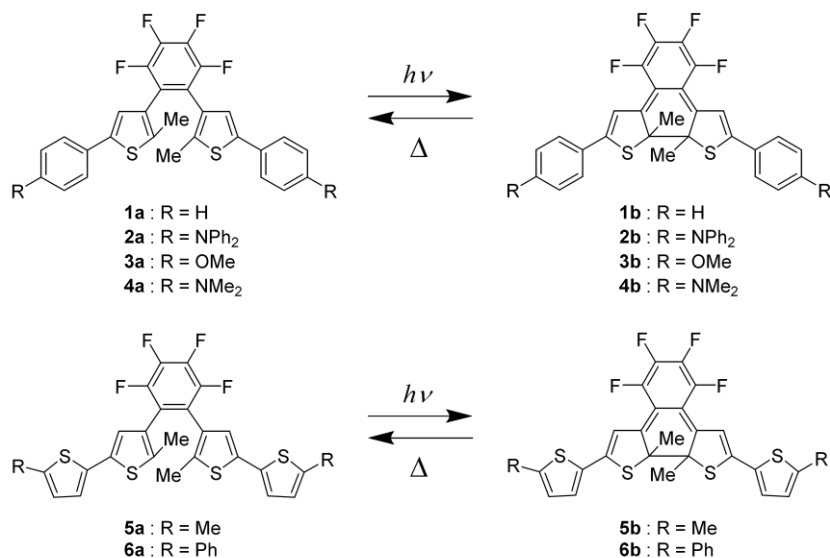
ABSTRACT

1,2-Diarylbenzenes (DABs) have been developed as a new family of fast T-type photochromic switches. However, the molecular design strategy for the DAB having desired optical and thermal properties is not established. In this work, we explored the best functional in the quantum chemical calculations to predict the properties of DABs. Furthermore, we newly designed and synthesized DABs based on the calculation with the best functional, resulting in the improvement of the photosensitivity in the UV-A region (i.e. a shift of absorption to lower energies and an increase absorption coefficient) without changing the thermal back-reaction rate.

Introduction

T-type photochromic compounds exhibiting a fast thermal back-reaction with a half-life ($t_{1/2}$) of a few seconds or below at room temperature, *i.e.* fast T-type photochromic compounds, have attracted much attention for application to ophthalmic lenses,¹ real-time holography,^{2, 3} super-resolution fluorescence microscopy,^{4, 5} photoactuators,^{6, 7} and so on. Oxazine,⁸⁻¹¹ naphthopyran,^{1, 12} hexaarylbiimidazole (HABI),¹³⁻¹⁵ and phenoxy-imidazolyl radical complex^{15, 16} have been reported as the fast T-type photochromic compounds so far. Although these chromophores have excellent properties such as tunability of the thermal back-reaction rate of photogenerated colored isomers and high fatigue resistance, there are drawbacks such as a deactivation by the influence of oxygen and a decrease of the photochromic reactivity in a solid phase due to a large molecular structural change during the photoisomerization. Exploration of a novel fast T-type photochromic system with excellent properties is still attracting much attention. Under this background, a fast T-type photochromic system based on 6π -electron photocyclization/thermal cycloreversion still has the potential to develop. Diarylethene (DAE) is one of the representative P-type photochromic compounds and has excellent photochromic properties such as rapid response, high durability, high sensitivity, reactivity in the solid-state.¹⁷ Moreover, it is known that DAE can be transformed into a T-type photochrome based on 6π -electron photocyclization/thermal cycloreversion by introducing various substituents.¹⁸⁻²⁴ Inspired by these excellent works, recently, we have developed a novel fast T-type photochromic 1,2-diarylbenzene (DAB) molecule, 1,2-bis(2-methyl-5-phenyl-3-thienyl)tetrafluorobenzene (**1a**), by only introducing a tetrafluorophenyl ring to the ethene bridge of a DAE molecule, 1,2-bis(2-methyl-5-phenyl-3-thienyl)perfluorocyclopentene.²⁵ DABs would be one of the most promising compounds as a new family of the fast T-type photochromic switches with the excellent properties as well as DAEs.

However, **1a** has a drawback to be unable to absorb the light with wavelengths longer than ~330 nm. Improving the photosensitivity in the UV-A region is strongly required for the practical applications such as ophthalmic lenses. Very recently, we have developed DABs (**2a-4a**) bearing various electron-donating groups at the *p*-position of the lateral phenyl ring with the aim of increasing the photosensitivity in the UV-A region.²⁶ DABs **2a-4a** exhibited red-shifted absorption spectra and higher absorption coefficients compared with those of **1a**. In this case, we have succeeded in increasing the photosensitivity in the UV-A region, but the thermal back-reaction rate was also affected by the substitution. The rate constants of the thermal back-reaction were correlated with the electron-donating ability of the substituent and the $t_{1/2}$ at 298 K changed from 130 ms to 1140 ms by introducing dimethylamino group. Hence, the strategy for the molecular design to increase the photosensitivity in the UV-A region of DAB without changing the thermal back-reaction rate is required. Here, we newly designed and synthesized DABs **5a** and **6a** having aryl groups with longer π -conjugation (Scheme 1). The optical properties and thermal reactivities were investigated.



Scheme 1. 1,2-Diarylbzenes used in this work.

Experimental Section

General

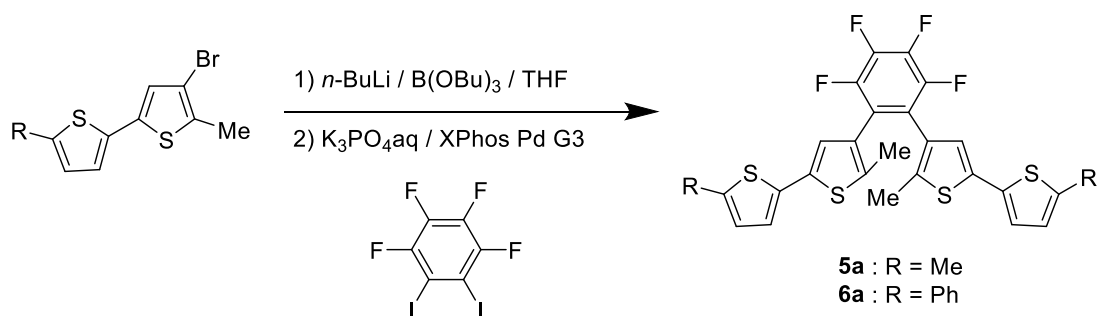
All the solvents used were of spectroscopic grade and/or purified by distillation before use. ^1H NMR (300 MHz) and ^{13}C NMR (75 MHz) spectra were measured using a Bruker AV-300N spectrometer with tetramethylsilane as the internal standard. High-resolution mass spectra were recorded on a Bruker FT-ICR/solariX mass spectrometer. UV-Vis absorption spectra were obtained on a JASCO V-560 absorption spectrometer. The light power was measured using a Neoark PM-335A power meter.

Theoretical Studies

Geometry optimizations and frequency calculations of open-ring isomers (Open), closed-ring isomers (Closed), and transition states (TS) were conducted using Gaussian 09 Rev.C.01 program package.²⁷ The transition-state search was performed with Opt = TS keyword, using Berny algorithm to optimize to a transition state. Each stationary point was identified by the number of imaginary frequencies ($N_{\text{Imag}} = 1$ for transition state and $N_{\text{Imag}} = 0$ for the local minimum) and by zero-point vibrational energies. To obey unrestricted Kohn–Sham solution, the broken-symmetry guess was generated and followed using keyword Guess (mix, always). Density functional theory (DFT) calculation was carried out using various functionals (B3LYP,²⁸⁻³⁰ BMK,³¹ M05,³² M05-2X,³³ M06,³⁴ M06-2X,³⁴ ω B97X-D³⁵) in combination with a 6-31G(d) or 6-31G(d,p) basis set.³⁶ Time dependent (TD)-DFT calculation was performed using various functionals (B3LYP, BMK, M05, M05-2X, M06, M06-2X, ω B97X-D, CAM-B3LYP,³⁷ MPW1DW91³⁸) with the optimized molecular structures at the M06-2X/6-31G(d) level.

Materials

Chemicals used for the syntheses were commercially available and used without further purification. DABs **1a-4a** were prepared by a procedure reported previously.^{25, 26} The synthetic procedure of **5a** and **6a** is shown in Scheme 2.



Scheme 2. Synthetic procedure of **5a** and **6a**.

1,2-Bis(2-methyl-5-(5-methyl-2-thienyl)-3-thienyl)tetrafluorobenzene (5a). 3-Bromo-2-methyl-5-(5-methyl-2-thienyl)thiophene³⁹ (410 mg, 1.5 mmol) was dissolved in dry THF (20 mL) under argon atmosphere. 1.6 M *n*-BuLi hexane solution (1.2 mL, 1.9 mmol) was slowly added dropwise to the solution at -78 °C, and the mixture was stirred for 1 h. Tri-*n*-butyl borate (0.9 mL, 3.4 mmol) was slowly added to the solution, and the mixture was further stirred at -78 °C for 2 h. The reaction was quenched by the addition of water. 1,2-Diodotetrafluorobenzene (110 mg, 0.27 mmol), XPhos Pd G3 (24 mg, 0.028 mmol), and 0.5 M K₃PO₄ (5.8 mL) were added to the reaction mixture, and the mixture was refluxed for 5 h. The reaction mixture was neutralized by HCl aqueous solution, extracted with ether, dried over MgSO₄, filtered, and concentrated. The crude

product was purified by column chromatography on silica gel (*n*-hexane/ethyl acetate = 95:5) and by HPLC (*n*-hexane/ethyl acetate = 98:2) to give 62 mg of **5a** in 42% yield based on 1,2-diiidotetrafluorobenzene. **5a**: ¹H NMR (300 MHz, CDCl₃, TMS) δ = 2.09-2.21 (br, 6H, CH₃), 2.43 (s, 6H, CH₃), 6.46-6.59 (br, 4H, Aromatic H), 6.79 (s, 2H, Aromatic H). ¹³C NMR (75 MHz, CDCl₃) δ = 13.9, 15.4, 120.8, 123.5, 125.1, 125.9, 128.2, 134.3, 134.7, 139.2. HR-MS (MALDI) *m/z* = 534.0223 (M⁺). Calcd for C₂₆H₁₈F₄S₄⁺ = 534.0222.

1,2-Bis(2-methyl-5-(5-phenyl-2-thienyl)-3-thienyl)tetrafluorobenzene (6a). 3-Bromo-2-methyl-5-(5-phenyl-2-thienyl)thiophene⁴⁰ (600 mg, 1.8 mmol) was dissolved in dry THF (20 mL) under argon atmosphere. 1.6 M *n*-BuLi hexane solution (1.4 mL, 2.2 mmol) was slowly added dropwise to the solution at -78 °C, and the mixture was stirred for 1.5 h. Tri-*n*-butyl borate (1.0 mL, 3.7 mmol) was slowly added to the solution, and the mixture was further stirred at -78 °C for 1.5 h. The reaction was quenched by the addition of water. 1,2-Diiidotetrafluorobenzene (140 mg, 0.35 mmol), XPhos Pd G3 (31 mg, 0.037 mmol), and 0.5 M K₃PO₄ (7.2 mL) were added to the reaction mixture, and the mixture was refluxed for 6 h. The reaction mixture was neutralized by HCl aqueous solution, extracted with ether, dried over MgSO₄, filtered, and concentrated. The crude product was purified by column chromatography on silica gel (*n*-hexane/ethyl acetate = 95:5) to give 80 mg of **6a** in 35% yield based on 1,2-diiidotetrafluorobenzene. **6a**: ¹H NMR (300 MHz, CDCl₃, TMS) δ = 2.14-2.25 (br, 6H, CH₃), 6.59-6.75 (br, 2H, Aromatic H), 6.99 (s, 2H, Aromatic H), 7.16-7.53 (m, 12H, Aromatic H). ¹³C NMR (75 MHz, CDCl₃) δ = 14.0, 120.7, 123.7, 124.6, 125.7, 127.7, 128.4, 129.0, 134.0, 134.1, 136.3, 138.0, 143.3. HR-MS (MALDI) *m/z* = 658.0535 (M⁺). Calcd for C₃₆H₂₂F₄S₄⁺ = 658.0535.

Photochromic Reaction

The measurement of transient absorption spectra of the closed-ring isomers at room temperature were performed using a Nikon ECLIPSE E600 optical microscope equipped with Ocean Optics USB4000 fiber multichannel analyzer as the photodetector. Photoirradiation was carried out using a 200 W mercury–xenon lamp (MORITEX MSU-6) as the light source. Monochromatic light was obtained by passing the light through a band-pass filter.

Thermal Back-Reaction

The thermal back-reaction of DAB closed-ring isomers was observed in tetrahydrofuran (THF). The DAB open-ring isomers were dissolved in THF. The solution in an optical quartz cuvette was irradiated with 313 nm light prepared by passing light from a 300W xenon lamp (Asahi Spectra MAX-301) through a band-pass filter to give the closed-ring isomers at the temperature of measurement. The cuvette was placed in a cryostat for spectroscopic measurements (UNISOKU CoolSpek UV/CD) during the measurement.

Results and Discussion

Selection of the Best Functional in DFT Calculation to Predict Properties of DABs

First of all, to perform accurate molecular design by DFT calculation, we started by finding the most suitable functional that well reproduces the experimental results. Masunov *et al.* previously reported that B3LYP and M05-2X are the best functionals to describe the kinetics of the thermal cycloreversion in DAEs and the use of unrestricted broken-symmetry DFT formalism is required for the calculation of the transition state because of the strong diradical character.⁴¹ According to this previous study,⁴¹⁻⁴³ here, we performed geometry optimizations and harmonic frequency calculations of the closed-ring isomer and transition state of **1** at various theories (Table 1). The activation energy (E_a) was calculated as the difference in sum of electronic and zero-point energies between the closed-ring isomer and the transition state. Figure 1a shows the differences in E_a between the estimated value by DFT calculation and the experimental one, i.e. $\Delta E_a = E_{a(\text{calcd})} - E_{a(\text{exp})}$. The B3LYP, M06, M05, and ω B97X-D functionals significantly underestimated the E_a value, while BMK functional overestimated it. On the other hand, the $E_{a(\text{calcd})}$ of **1** (63.22 kJ mol⁻¹) estimated at the M05-2X/6-31G(d) level is close to the $E_{a(\text{exp})}$ (66 kJ mol⁻¹), which is the same trend as the results reported by Masunov *et al.*⁴¹ This indicates that the M05-2X functional gives the good prediction for the thermal back reactivity of DAB as well as DAE. Furthermore, the $E_{a(\text{calcd})}$ estimated at the M06-2X/6-31G(d) level was 66.64 kJ mol⁻¹, which is the closest values to the $E_{a(\text{exp})}$ among those calculated in this work. In addition, it was revealed that the $E_{a(\text{calcd})}$ value hardly changed even when the basis set was changed from 6-31G(d) to 6-31G(d,p). To confirm whether the M06-2X functional gives a $E_{a(\text{calcd})}$ close to the $E_{a(\text{exp})}$ value even on the other DABs, the $E_{a(\text{calcd})}$ of **2-4** whose $E_{a(\text{exp})}$ values were reported previously were also calculated.²⁶ The $E_{a(\text{calcd})}$ of **2-4** were estimated to be 67.75, 70.17, and 73.56 kJ mol⁻¹, respectively, which are much closer

values to the $E_{a(\text{exp})}$ compared with those calculated at the B3LYP/6-31G(d) reported previously (Table 1).²⁶ The errors between $E_{a(\text{calcd})}$ and $E_{a(\text{exp})}$ (ΔE_a) were within 3.5 kJ mol⁻¹. In the previous work on photochromic diarylethenes reported by Masunov *et al.*,⁴¹ the ΔE_a was 12.6–16.7 kJ mol⁻¹ even with the best functional of B3LYP and M05-2X. Thus, we have found a functional that allows more accurate prediction of the thermal reactivity of diarylbenzenes. Considering the results so far, we adopted the M06-2X as the functional to perform the geometry optimizations and the harmonic frequency calculations.

Table 1. $E_{a(\text{calcd})}$ values for the thermal back-reaction of **1-4** calculated at various theories.

Compound	Functional /Basis Set	Energy (Closed) /hartree	Energy (TS) /hartree	$E_{a(\text{calcd})}$ /kJ mol ⁻¹	ΔE_a /kJ mol ^{-1a}
1 $E_{a(\text{exp})}$ = 66 kJ mol ^{-1b}	B3LYP/6-31G(d) ^b	-2273.105085	-2273.083204	57.45	-8.55
	BMK/6-31G(d)	-2271.998186	-2271.970946	71.52	5.52
	M05/6-31G(d)	-2272.187491	-2272.173520	36.68	-29.32
	M05-2X/6-31G(d)	-2272.947053	-2272.922974	63.22	-2.78
	M06/6-31G(d)	-2272.132048	-2272.110497	56.58	-9.42
	M06-2X/6-31G(d)	-2272.469528	-2272.444146	66.64	0.64
	ωB97X-D/6-31G(d)	-2272.607807	-2272.588168	51.56	-14.44
M06-2X/6-31G(d,p)	-2272.492921	-2272.467528	66.67	0.67	
2 $E_{a(\text{exp})}$ = 69 kJ mol ^{-1c}	B3LYP/6-31G(d) ^c	-3307.650884	-3307.627547	61.27	-7.73
	M06-2X/6-31G(d)	-3306.595517	-3306.569713	67.75	-1.25
3 $E_{a(\text{exp})}$ = 71 kJ mol ^{-1c}	B3LYP/6-31G(d) ^c	-2502.087610	-2502.063988	62.02	-8.98
	M06-2X/6-31G(d)	-2501.361131	-2501.334404	70.17	-0.83
4 $E_{a(\text{exp})}$ = 77 kJ mol ^{-1c}	B3LYP/6-31G(d) ^c	-2540.898988	-2540.873679	66.45	-10.55
	M06-2X/6-31G(d)	-2540.138144	-2540.110127	73.56	-3.44

^a $\Delta E_a = E_{a(\text{calcd})} - E_{a(\text{exp})}$, ^bRef 25, ^cRef 26.

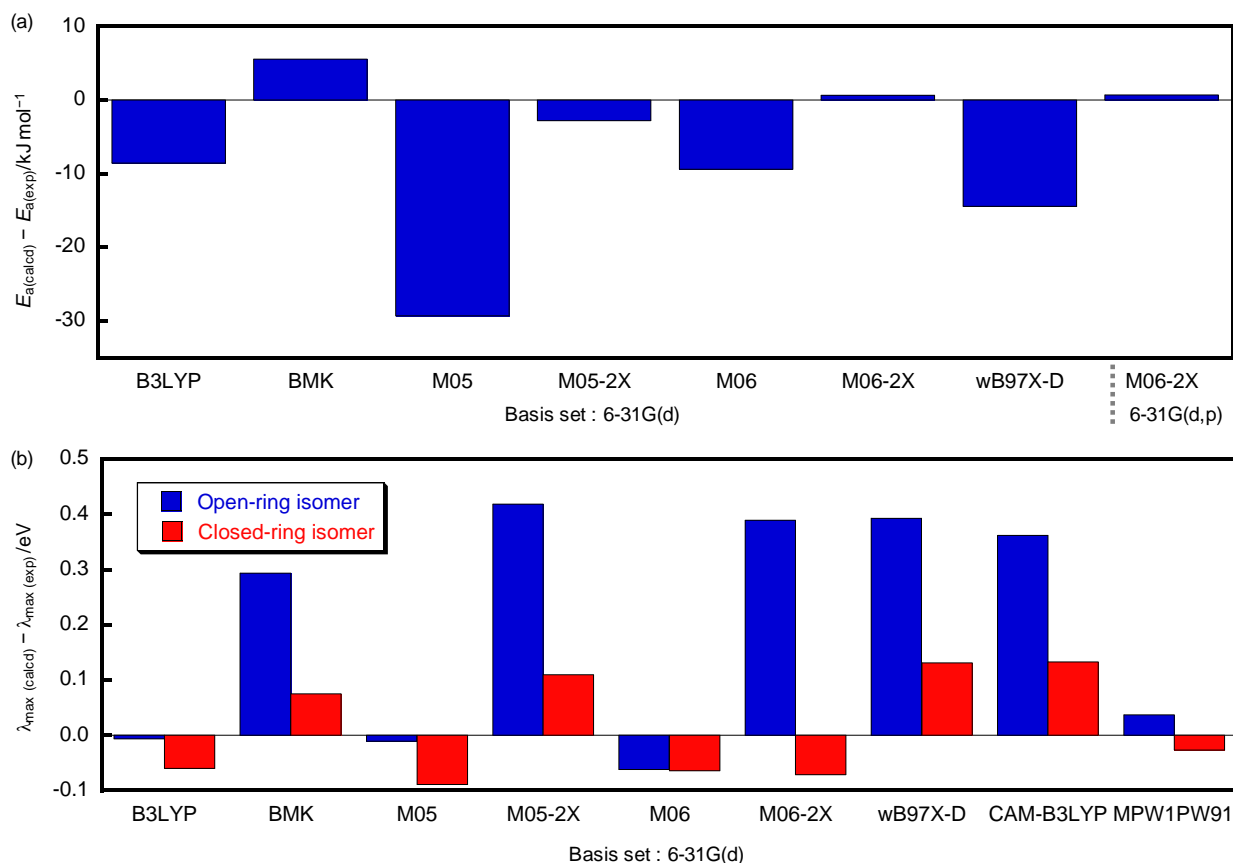


Figure 1. (a) The differences between the $E_{a(\text{calcd})}$ and $E_{a(\text{exp})}$ for **1** and (b) the differences between $\lambda_{\text{max}(\text{calcd})}$ and $\lambda_{\text{max}(\text{exp})}$ for **1**.

Furthermore, we also performed TD-DFT calculation using various theories with the optimized molecular structures at the M06-2X/6-31G(d) level to obtain the calculated absorption spectra that are close to the experimental ones. The results were listed in Table 2. Here, we defined the absorption maximum wavelength in the calculated absorption spectra as $\lambda_{\text{max}(\text{calcd})}$. For comparison, the $\lambda_{\text{max}(\text{calcd})}$ estimated by the CAM-B3LYP/6-31G(d)//B3LYP/6-31G(d) level used in our previous work was also listed. As shown in Figure 1b, most of the $\lambda_{\text{max}(\text{calcd})}$ values for the open- and closed-ring isomers differed from the experimental absorption maximum wavelength

($\lambda_{\max(\text{exp})}$) by 0.05 eV or more. On the other hand, $\lambda_{\max(\text{calcd})}$ of **1a** and **1b** estimated by at the MPW1PW91/6-31G(d) level were 4.388 and 1.672 eV, respectively, which were very close to the $\lambda_{\max(\text{exp})}$ (4.351 eV for **1a** and 1.699 eV for **1b**). In addition, the $\lambda_{\max(\text{calcd})}$ of **2-4** did not greatly differ from the $\lambda_{\max(\text{exp})}$ as well as **1**. Therefore, we concluded that TD-DFT calculation at the MPW1PW91/6-31G(d)//M06-2X/6-31G(d) level is the best choice to predict the absorption spectral properties of DABs.

Table 2. Absorption maximum wavelength ($\lambda_{\max(\text{calcd})}$) of **1-4** calculated by TD-DFT.

Compound	Functional/Basis Set	$\lambda_{\max(\text{calcd})}$ /nm (Open)	$\Delta\lambda_{\max}$ /eV (Open) ^a	$\lambda_{\max(\text{calcd})}$ /nm (Closed)	$\Delta\lambda_{\max}$ /eV (Closed) ^a
1 $\lambda_{\max(\text{exp})} = 285 \text{ nm}^b$ (4.351 eV) (Open) $\lambda_{\max(\text{exp})} = 730 \text{ nm}^b$ (1.699 eV) (Closed)	CAM-B3LYP/6-31G(d) ^c	269.2 (4.606 eV)	0.2554	757.9 (1.636 eV)	-0.0625
	B3LYP/6-31G(d)	285.4 (4.345 eV)	-0.0061	756.8 (1.638 eV)	-0.0602
	BMK/6-31G(d)	267.0 (4.644 eV)	0.2933	699.0 (1.774 eV)	0.0753
	M05/6-31G(d)	285.7 (4.340 eV)	-0.0107	770.4 (1.610 eV)	-0.0891
	M05-2X/6-31G(d)	260.0 (4.769 eV)	0.4183	685.8 (1.808 eV)	0.1095
	M06/6-31G(d)	289.1 (4.289 eV)	-0.0617	758.7 (1.634 eV)	-0.0643
	M06-2X/6-31G(d)	261.6 (4.740 eV)	0.3892	762.1 (1.627 eV)	-0.0715
	ω B97X-D/6-31G(d)	261.4 (4.744 eV)	0.3928	677.8 (1.829 eV)	0.1308
	CAM-B3LYP/6-31G(d)	263.1 (4.713 eV)	0.3622	677.1 (1.831 eV)	0.1327
MPW1PW91/6-31G(d)	282.6 (4.388 eV)	0.0369	741.6 (1.672 eV)	-0.0266	
2 $\lambda_{\max(\text{exp})} = 345 \text{ nm}^d$ (3.594 eV) (Open) $\lambda_{\max(\text{exp})} = 770 \text{ nm}^d$ (1.610 eV) (Closed)	CAM-B3LYP/6-31G(d) ^c	318.5 (3.893 eV)	0.2990	793.4 (1.563 eV)	-0.0475
	MPW1PW91/6-31G(d)	352.5 (3.518 eV)	-0.0765	772.8 (1.605 eV)	-0.0058
3 $\lambda_{\max(\text{exp})} = 290 \text{ nm}^d$ (4.276 eV) (Open) $\lambda_{\max(\text{exp})} = 735 \text{ nm}^d$ (1.687 eV) (Closed)	CAM-B3LYP/6-31G(d) ^c	274.8 (4.512 eV)	0.2365	760.4 (1.687 eV)	-0.0564
	MPW1PW91/6-31G(d)	286.4 (4.330 eV)	0.0537	740.7 (1.674 eV)	-0.0130
4 $\lambda_{\max(\text{exp})} = 315 \text{ nm}^d$ (3.936 eV) (Open) $\lambda_{\max(\text{exp})} = 765 \text{ nm}^d$ (1.621 eV) (Closed)	CAM-B3LYP/6-31G(d) ^c	293.3 (4.228 eV)	0.2912	777.8 (1.594 eV)	-0.0267
	MPW1PW91/6-31G(d)	303.9 (4.080 eV)	0.1438	754.5 (1.643 eV)	0.0226

^a $\Delta\lambda_{\max} = \lambda_{\max(\text{calcd})} - \lambda_{\max(\text{exp})}$. ^b $\lambda_{\max(\text{exp})}$ reported at ref 25. ^cGeometry optimization and harmonic frequency calculation were performed at the B3LYP/6-31G(d) level (ref 26). ^d $\lambda_{\max(\text{exp})}$ reported at ref 26

Molecular Design

Next, we moved on to the molecular design for the improvement of the photosensitivity in the UV-A region of DAB without changing the thermal back-reaction rate. To increase the photosensitivity in the UV-A region, extending the π -conjugation length is one of the representative strategies.⁴⁴ For example, in the case of DAE, replacing the lateral phenyl ring with a methylthiophene ring leads to a red-shift of the absorption spectrum because of a more effective conjugation, which is ascribed to both lower inter-ring torsional angles and less aromaticity of thienyl with respect to phenyl.⁴⁵ Moreover, a larger red-shift of the absorption spectrum can be induced by increasing the number of thiophene rings.⁴⁰ To know if the strategy is effective in the case of DABs, the absorption spectra for **5a** and **6a** were predicted by TD-DFT calculation. Figure 2 shows the predicted absorption spectra of **5a** and **6a** by TD-DFT calculation (MPW1PW91/6-31G(d)//M06-2X/6-31G(d) level of the theory). For comparison, the absorption spectrum of **1a** was also calculated. The results are summarized in Table S1. The $\lambda_{\max(\text{calcd})}$ for **5a** and **6a** were estimated at 302.6 and 348.6 nm, respectively, suggesting that the absorption spectra of **5a** and **6a** are red-shifted with respect to that of **1a** ($\lambda_{\max(\text{calcd})} = 282.6$ nm). In addition, the maximum oscillator strength (f) values of **5a** and **6a** were calculated to be 0.697 and 1.273, respectively, while that of **1a** was 0.649. This result suggests that the absorption coefficient of **5a** would be similar to that of **1a**, but that of **6a** would be much larger. This is due to the extension of π -conjugation by introducing phenyl group instead of methyl group. As can be seen in Figure 3b, the π -orbitals for HOMO \rightarrow LUMO and HOMO-1 \rightarrow LUMO+1, which are contributions of the transition at $\lambda_{\max(\text{calcd})}$ for **6a**, greatly overlap. Summing up these results of calculations, the photosensitivity in the UV-A region for **5a** and **6a** would be increased compared with that for **1a**. However, here, one should notice that the reactivity of DAB is also related to the phase of the

reactive carbons at the orbitals contributing to the electronic transition.⁴⁶ Although the TD-DFT calculations do not directly provide information about the potential energy surface of photoexcited states, the results would be useful to know the possibility of the photoreaction. Based on the Woodward-Hoffmann rules, the photochromic reaction of DAB proceeds photochemically through a conrotatory mechanism. If the phase of the reactive carbons at the orbitals contributing to the electronic transition is the anti-phase, DAB cannot undergo the photocyclization even when there is the absorption band in the UV-A region. To investigate the phase of the reactive carbons at the orbitals contributing to the electronic transition, we checked the contributions of the configurations for the electronic transition at $\lambda_{\text{max(calcd)}}$. The outputs of the TD-DFT calculations for **5a** and **6a** were shown in Table S2. In the case of **5a**, the transition at $\lambda_{\text{max(calcd)}}$ was assigned to the contributions of HOMO→LUMO+2, HOMO-1→LUMO+1, and HOMO→LUMO configurations. The molecular orbitals related to the transitions were shown in Figure 3a. The LUMO orbital only has the same phase at the reactive carbons and allows the photocyclization, while both LUMO+1 and LUMO+2 orbitals have the anti-phase at the two reactive carbons. In addition, the transition at $\lambda_{\text{max(calcd)}}$ for **6a** mainly corresponded to HOMO→LUMO configuration. The LUMO orbitals have the same phase at the reactive carbons as shown in Figure 3b. As a result, it is assumed that **5a** and **6a** can undergo the photocyclization by the contribution of the HOMO→LUMO configuration.

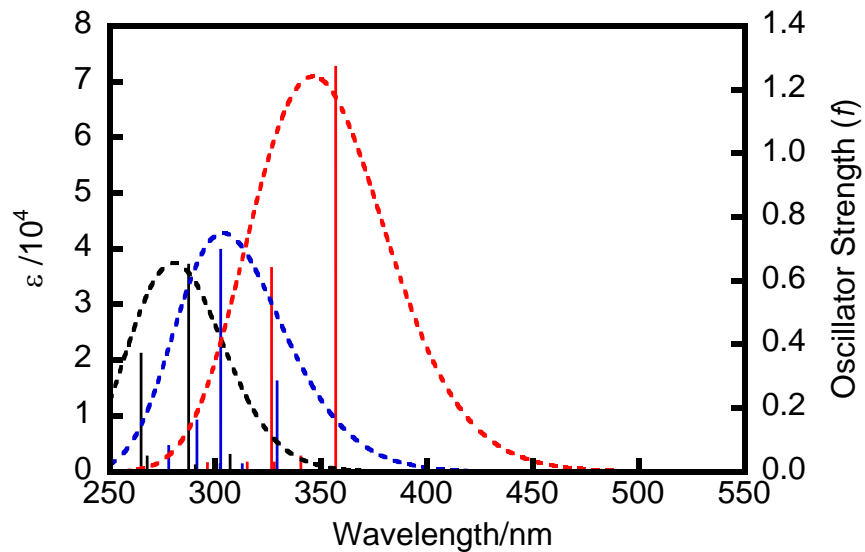


Figure 2. Calculated absorption spectra of **1a** (black), **5a** (blue), and **6a** (red) by TD-DFT (MPW1PW91/6-31G(d)//M06-2X/6-31G(d) level of the theory), modeled with a half width at half-maximum (HWHM) of 2000 cm^{-1} .

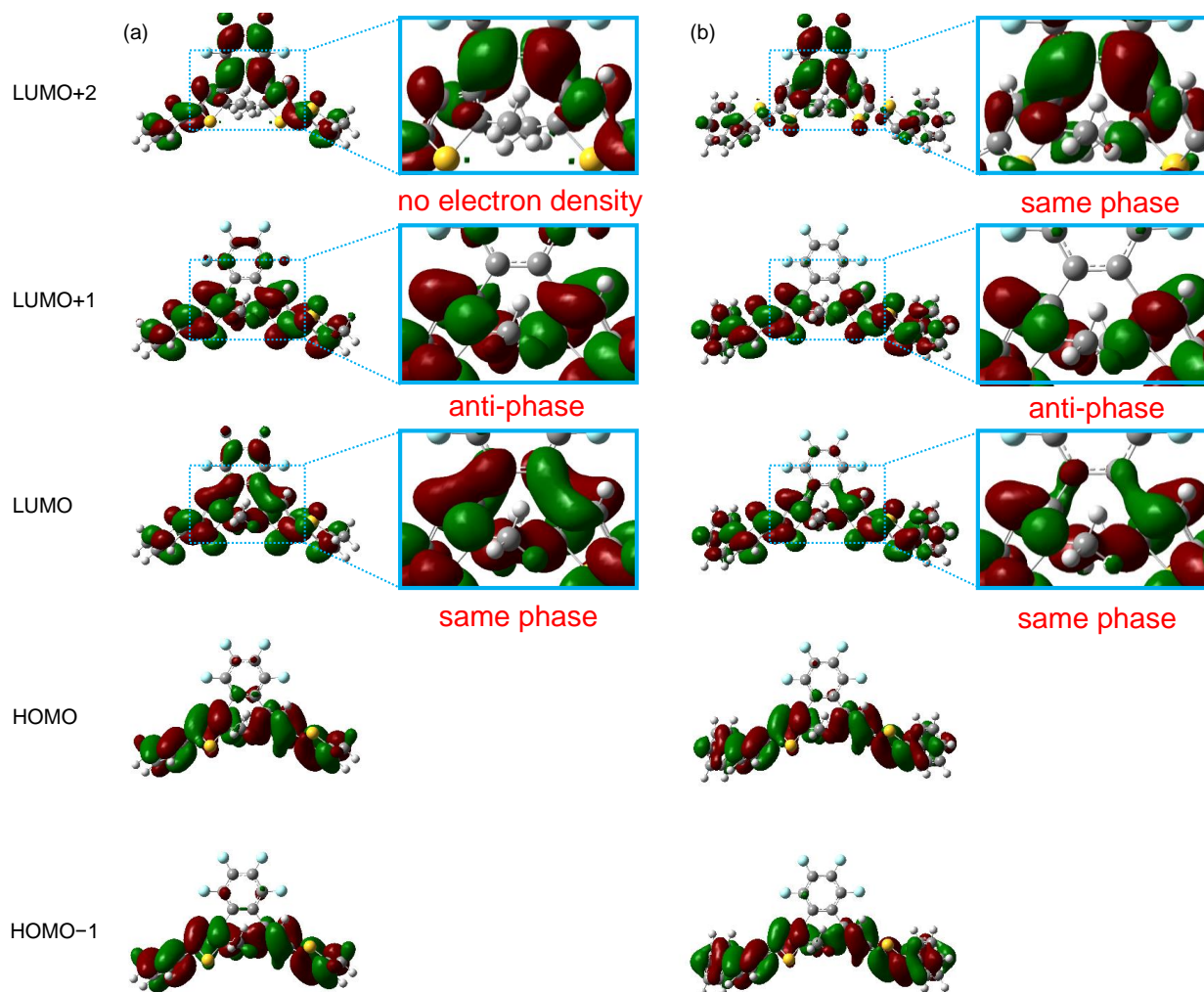


Figure 3. Relevant molecular orbitals of (a) **5a** and (b) **6a** obtained at the M06-2X/6-31G(d) level.

Next, we tried to predict the thermal reactivity of **5b** and **6b**. To estimate the thermal reactivity of **5b** and **6b**, the $E_{a(\text{calcd})}$ for **5** and **6** were calculated by DFT at the M06-2X/6-31G(d) level. The calculated values are summarized in Table 3. The values for **1** were also listed for comparison. The $E_{a(\text{calcd})}$ values for **5** and **6** were 69.10 and 66.38 kJ mol⁻¹, respectively. The values are almost the same as that for **1** (66.64 kJ mol⁻¹). These calculations imply that extending the π -

conjugation length would increase the photosensitivity in the UV-A region, though the thermal reactivity would not be changed much. This is just the molecular design that we were looking for.

Table 3. $E_{a(\text{calcd})}$ for the thermal back-reaction and energy gap (ΔE) between the open- and closed-ring isomers calculated by DFT (M06-2X/6-31G(d) level of the theory).

	Energy (Open) /hartree	Energy (Closed) /hartree	Energy (TS) /hartree	$E_{a(\text{calcd})}$ /kJ mol ^{-1a}	ΔE /kJ mol ^{-1b}
1	-2272.513804	-2272.469528	-2272.444146	66.64	116.25
5	-2992.637777	-2992.598719	-2992.572402	69.10	102.55
6	-3375.86078	-3375.821669	-3375.796388	66.38	102.69

^a $E_{a(\text{calcd})}$ = Energy (TS) – Energy (Closed). ^b ΔE = Energy (Closed) – Energy (Open).

Photochromic Reaction

To confirm the validity of the molecular design strategy described above, **5a** and **6a** were synthesized. The synthetic procedures were described in Scheme 2 and Experimental Section. Figure 4 shows the absorption spectra of **5a** and **6a** in THF. For comparison, the absorption spectrum of **1a** was also shown. The optical and thermal properties of **1**, **5**, and **6** are summarized in Table 4. As can be seen, the absorption spectra of **5a** and **6a** were red-shifted in comparison with that of **1a**. The $\lambda_{\text{max}(\text{exp})}$ of **5a** and **6a** were 312 and 345 nm, respectively. The $\lambda_{\text{max}(\text{exp})}$ was red-shifted by 25 nm for **5a** and 58 nm for **6a** compared with that for **1a**. In addition, the absorption coefficients at $\lambda_{\text{max}(\text{exp})}$ (ϵ_{max}) for **5a** and **6a** were determined to be 28900, and 47000 M⁻¹ cm⁻¹, respectively. The ϵ_{max} of **6a** is much higher than that of **1a** ($\epsilon_{\text{max}} = 30600$ M⁻¹ cm⁻¹). These results are consistent with the prediction by DFT calculations mentioned above.

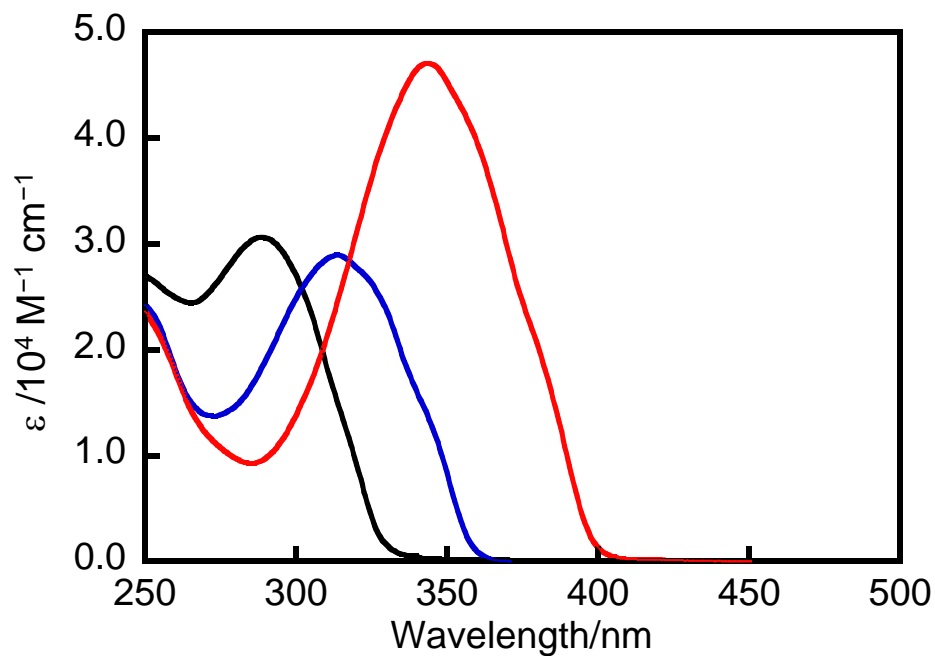


Figure 4. Absorption spectra of **1a** (black), **5a** (blue) and **6a** (red) in THF.

Table 4. Optical properties and Arrhenius parameters for the thermal back-reaction of DABs in THF.

	Open		Closed	$E_{a(\text{exp})}$ /kJ mol ⁻¹	A/s^{-1}	k/s^{-1} at 298 K	$t_{1/2}/\text{ms}$ at 298 K
	$\lambda_{\text{max}(\text{exp})}/\text{nm}$	$\epsilon_{\text{max}}/\text{M}^{-1} \text{cm}^{-1}$	$\lambda_{\text{max}(\text{exp})}/\text{nm}$				
1	287	30600	725	62	7.0×10^{11}	8.2	84
5	312	28900	755	67	1.6×10^{12}	2.5	280
6	345	47000	790	63	7.7×10^{11}	7.7	90

Upon irradiation with 313 nm light, **5a** and **6a** isomerized to **5b** and **6b**, which were detected by the absorption spectra in visible region as shown in Figure S1. The colorless solutions of **5a** and **6a** turned green only while the solutions are irradiated with UV light. This is due to the fast thermal back-reaction. The $\lambda_{\max(\text{exp})}$ of **5b** and **6b** were 755 and 790 nm, respectively, which are red-shifted by 30 nm for **5b** and 65 nm for **6b** compared with that of **1b** (Figure S2). This is also consistent with the UV-vis spectra predicted by TD-DFT calculation for **5b** and **6b** (MPW1PW91/6-31G(d)//M06-2X/6-31G(d) level of the theory) (Figure S3 and Table S3). The red-shift in the absorption spectra of **5b** and **6b** was due to a decrease in highest occupied molecular orbital (HOMO)–lowest unoccupied molecular orbital (LUMO) gap by extending π -conjugation. The HOMO–LUMO gap for **1b** was -0.1283 eV, though those for **5b** and **6b** were -0.1229 and -0.1191 eV, respectively (Table S4).

To know if the photochromic reaction can be induced by UV-A light (365 nm), the absorption spectral changes for **5a** and **6a** upon irradiation with 365 nm light were also observed. Figure 5 shows the absorption spectra of **5a** and **6a** irradiated by 365 nm light. The absorption bands assigned to the photogenerated isomers **5b** and **6b** were confirmed in the visible region even when 365 nm light was used for the incident light. This result indicates that the photosensitivity in the UV-A region was successfully improved by extending π -conjugation.

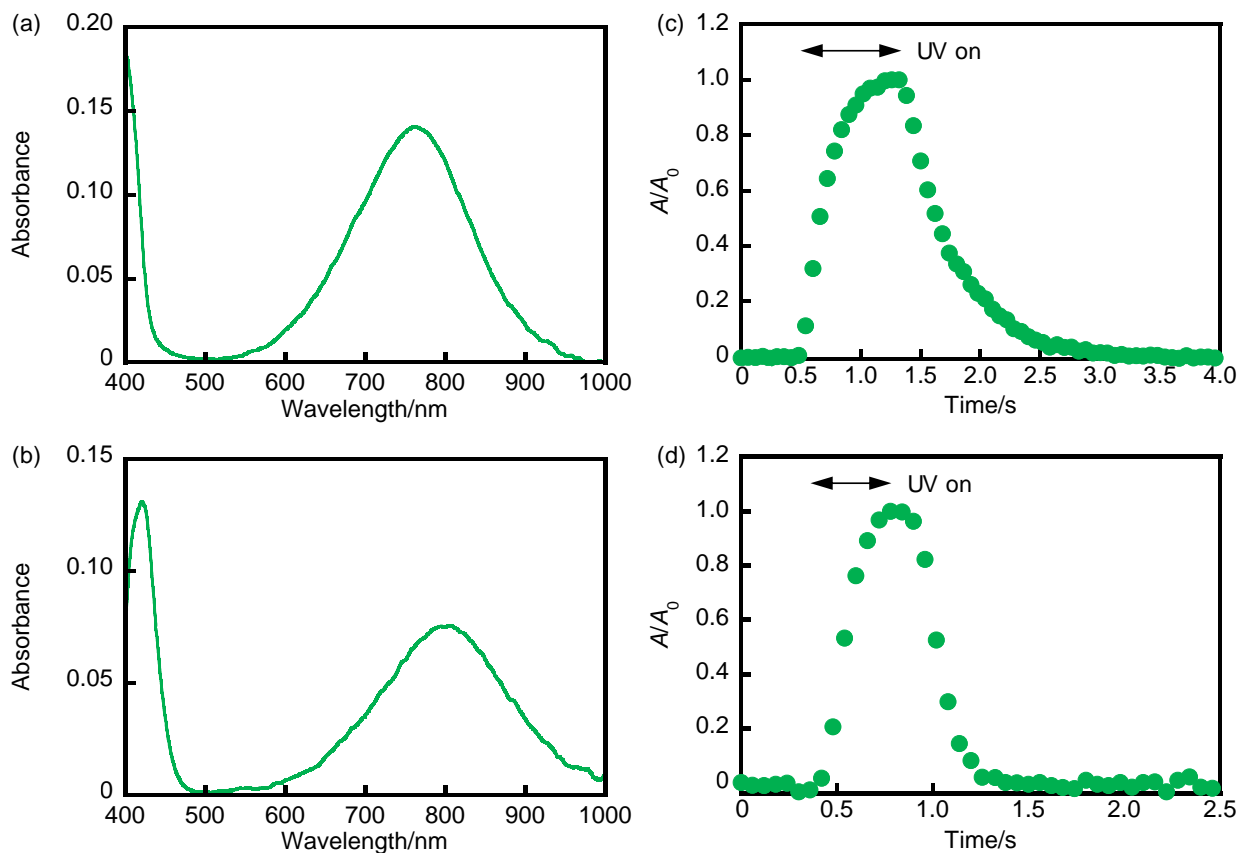


Figure 5. Absorption spectra of (a) **5b** ($[5a] = 8.7 \times 10^{-4} \text{ M}$) and (b) **6b** ($[6a] = 4.2 \times 10^{-5} \text{ M}$) in THF upon irradiation with 365 nm light (100 mW cm^{-2}) at 298 K and absorbance change of (c) **5b** and (d) **6b** in THF relative to time upon irradiation with 365 nm light (100 mW cm^{-2}) for 0.6 s (**5b**) and 0.3 s (**6b**), and thermal bleaching at 298 K. The data points of each absorbance were averaged over the data from 740 to 770 nm (**5b**) and from 775 to 805 nm (**6b**) and were recorded at 60 ms intervals for **5b** and **6b**.

Analysis of Thermal Back-Reaction

Another important factor of the fast T-type photochromic molecules is the thermal reactivity. The purpose in this work is to improve the photosensitivity in the UV-A region without

changing the thermal reactivity. To get insights into the thermal reactivity of **5b** and **6b**, the change in the absorption of **5b** and **6b** as a function of time at various temperatures was recorded. Figure 6a and b show absorption decay curves at $\lambda_{\text{max}(\text{exp})}$ for **5b** and **6b**. The thermal back-reaction proceeded to follow first-order kinetics. The rate constants (k) at various temperatures were determined from the slope of the first-order plots (Tables S5 and S6). The temperature dependences of k for **5b** and **6b** were shown in Figure 6c and d. The $E_{\text{a}(\text{exp})}$ values and the frequency factor (A) of the thermal back-reaction were calculated from the slope and intercept of the linear Arrhenius plots. For comparison, the absorption decay curves at $\lambda_{\text{max}(\text{exp})}$ for **1b** were also examined (Figure S4 and Table S7). The results are summarized in Table 4 with the data of **1b**. The $E_{\text{a}(\text{exp})}$ values of **5b** and **6b** were 67 and 63 kJ mol^{-1} , respectively, which are very similar to that of **1b** (62 kJ mol^{-1}). The $E_{\text{a}(\text{exp})}$ values are consistent with the $E_{\text{a}(\text{calcd})}$ values predicted by DFT calculation. The A values for **5b** and **6b** were estimated to be 1.6 and $0.77 \times 10^{12} \text{ s}^{-1}$, respectively. The $t_{1/2}$ of **5b** and **6b** at 298 K were calculated to be 280 and 90 ms, respectively, which are comparable to that of **1b** (84 ms). Moreover, the Eyring plot was also performed to estimate the ΔH^\ddagger , ΔS^\ddagger , and ΔG^\ddagger values as shown in Figures S5–S7 and the results are summarized in Table S8. The ΔH^\ddagger , ΔS^\ddagger , and ΔG^\ddagger values for **1**, **5**, and **6** hardly changed and are comparable to that for a HABI derivative.¹⁴ Thus, DABs **5** and **6** synthesized in this work exhibited not only the improved photosensitivity but also the desired thermal back-reaction rate as predicted by the DFT calculations. These results would provide the methodology to design the DABs having desired optical and thermal properties.

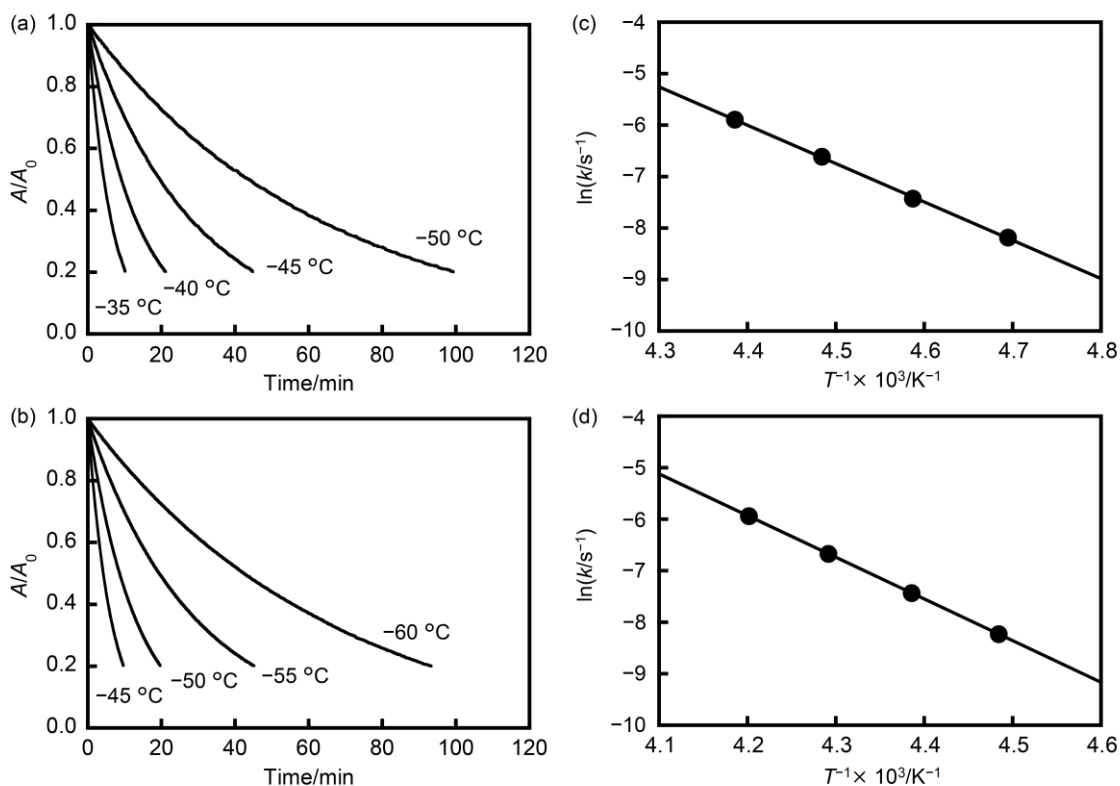


Figure 6. Absorption decay curves at $\lambda_{\max(\text{exp})}$ for (a) **5b** and (b) **6b** in THF at various temperatures and temperature dependence of the rate constant (k) for thermal back-reaction of (c) **5b** and (d) **6b**.

Conclusions

In this work, we have selected the best functional in DFT calculation to accurately predict the optical and thermal properties of DABs. Regarding the estimation of the activation energy of the thermal back-reaction of DABs by DFT calculation, the M06-2X level of theory in combination with a 6-31G(d) basis set was the best functional that well reproduces the experimental results. Furthermore, as for the prediction of the absorption spectra of DABs by TD-DFT calculation, the MPW1PW91 level of theory in combination with a 6-31G(d) basis set using the optimized

molecular structures at the M06-2X/6-31G(d) level was the best choice. Based on the calculation using the best functionals, DABs **5a** and **6a** having aryl groups with longer π -conjugation were designed and synthesized. The absorption spectra of **5a** and **6a** were red-shifted in comparison with that of **1a**. They showed a fast T-type photochromic reaction with the $t_{1/2}$ of 280 and 90 ms at 298 K even upon irradiation with UV-A (365 nm) light, while the $t_{1/2}$ were similar to that of **1a** ($t_{1/2} = 84$ ms). Thus, the improvement of the photosensitivity in the UV-A region without changing the thermal back-reaction rate could be accomplished. The results in this work provide useful information for the molecular design strategy of DABs having desired optical and thermal properties.

ASSOCIATED CONTENT

Electronic Supplementary Information (ESI) available: Detailed experimental data (Figures S1–S7 and Tables S1–S17).

AUTHOR INFORMATION

Corresponding Author

*Email: kitagawa@osaka-cu.ac.jp and kobatake@a-chem.eng.osaka-cu.ac.jp.

ORCID

Daichi Kitagawa: 0000-0002-1994-3047

Tatsumoto Nakahama: 0000-0002-0546-9305

Seiya Kobatake: 0000-0002-1526-4629

Notes

The authors declare no competing financial interest.

ACKNOWLEDGMENT

This work was partly supported by JSPS KAKENHI Grant Numbers JP26107013 in Scientific Research on Innovative Areas “Photosynergetics” (S. K.), JSPS KAKENHI Grant Number JP16K17896 in Scientific Research for Young Scientists B (D. K.) and JSPS KAKENHI Grant Number 18J10399 in Scientific Research for JSPS fellow (T. N.).

References

1. Y. Inagaki, Y. Kobayashi, K. Mutoh and J. Abe, A simple and versatile strategy for rapid color fading and intense coloration of photochromic naphthopyran families, *J. Am. Chem. Soc.*, 2017, **139**, 13429-13441.
2. Y. Kobayashi and J. Abe, Real-time dynamic hologram of a 3D object with fast photochromic molecules, *Adv. Opt. Mater.*, 2016, **4**, 1354-1357.
3. N. Ishii, T. Kato and J. Abe, A real-time dynamic holographic material using a fast photochromic molecule, *Sci. Rep.*, 2012, **2**, 819.
4. J. Cusido, S. S. Ragab, E. R. Thapaliya, S. Swaminathan, J. Garcia-Amorós, M. J. Roberti, B. Araoz, M. M. A. Mazza, S. Yamazaki, A. M. Scott, F. M. Raymo and M. L. Bossi, A photochromic bioconjugate with photoactivatable fluorescence for superresolution imaging, *J. Phys. Chem. C*, 2016, **120**, 12860-12870.

5. E. Deniz, M. Tomasulo, J. Cusido, I. Yildiz, M. Petriella, M. L. Bossi, S. Sortino and F. M. Raymo, Photoactivatable fluorophores for super-resolution imaging based on oxazine auxochromes, *J. Phys. Chem. C*, 2012, **116**, 6058-6068.
6. F. Tong, M. P. Hanson and C. J. Bardeen, Analysis of reaction kinetics in the photomechanical molecular crystal 9-methylanthracene using an extended Finke-Watzky model, *Phys. Chem. Chem. Phys.*, 2016, **18**, 31936-31945.
7. L. Zhu, F. Tong, C. Salinas, M. K. Al-Muhanna, F. S. Tham, D. Kisailus, R. O. Al-Kaysi and C. J. Bardeen, Improved solid-state photomechanical materials by fluorine substitution of 9-anthracene carboxylic acid, *Chem. Mater.*, 2014, **26**, 6007-6015.
8. M. Tomasulo, S. Sortino, A. J. P. White and F. M. Raymo, Fast and stable photochromic oxazines, *J. Org. Chem.*, 2005, **70**, 8180-8189.
9. M. Tomasulo, S. Sortino and F. M. Raymo, A fast and stable photochromic switch based on the opening and closing of an oxazine ring, *Org. Lett.*, 2005, **7**, 1109-1112.
10. M. Tomasulo, S. Sortino and F. M. Raymo, Amplification of the coloration efficiency of photochromic oxazines, *Adv. Mater.*, 2008, **20**, 832-835.
11. Y. Zhang, S. Tang, E. R. Thapaliya, L. Sansalone and F. M. Raymo, Fluorescence activation with switchable oxazines, *Chem. Commun.*, 2018, **54**, 8799-8809.
12. C. M. Sousa, J. Berthet, S. Delbaere, A. Polónia and P. J. Coelho, Fast color change with photochromic fused naphthopyrans, *J. Org. Chem.*, 2015, **80**, 12177-12181.
13. K. Fujita, S. Hatano, D. Kato and J. Abe, Photochromism of a radical diffusion-inhibited hexaarylbiimidazole derivative with intense coloration and fast decoloration performance, *Org. Lett.*, 2008, **10**, 3105-3108.
14. Y. Kishimoto and J. Abe, A fast photochromic molecule that colors only under UV light, *J.*

- Am. Chem. Soc.*, 2009, **131**, 4227-4229.
15. H. Yamashita, T. Ikezawa, Y. Kobayashi and J. Abe, Photochromic phenoxyl-imidazolyl radical complexes with decoloration rates from tens of nanoseconds to seconds, *J. Am. Chem. Soc.*, 2015, **137**, 4952-4955.
 16. T. Ikezawa, K. Mutoh, Y. Kobayashi and J. Abe, Thiophene-substituted phenoxyl-imidazolyl radical complexes with high photosensitivity, *Chem. Commun.*, 2016, **52**, 2465-2468.
 17. M. Irie, T. Fukaminato, K. Matsuda and S. Kobatake, Photochromism of diarylethene molecules and crystals: memories, switches, and actuators, *Chem. Rev.*, 2014, **114**, 12174-12277.
 18. K. Uchida, T. Matsuoka, K. Sayo, M. Iwamoto, S. Hayashi and M. Irie, Thermally reversible photochromic systems. photochromism of a dipyrrolylperfluorocyclopentene, *Chem. Lett.*, 1999, **28**, 835-836.
 19. S. Kawai, T. Nakashima, K. Atsumi, T. Sakai, M. Harigai, Y. Imamoto, H. Kamikubo, M. Kataoka and T. Kawai, Novel photochromic molecules based on 4,5-dithienyl thiazole with fast thermal bleaching rate, *Chem. Mater.*, 2007, **19**, 3479-3483.
 20. Y. H. Yang, Y. S. Xie, Q. Zhang, K. Nakatani, H. Tian and W. H. Zhu, Aromaticity-controlled thermal stability of photochromic systems based on a six-membered ring as ethene bridges: photochemical and kinetic studies, *Chem. Eur. J.*, 2012, **18**, 11685-11694.
 21. V. Z. Shirinian, A. G. Lvov, E. Y. Bulich, A. V. Zakharov and M. M. Krayushkin, Novel photochromic diarylethenes bearing an imidazole moiety, *Tetrahedron Lett.*, 2015, **56**, 5477-5481.
 22. D. Kitagawa and S. Kobatake, Strategy for molecular design of photochromic

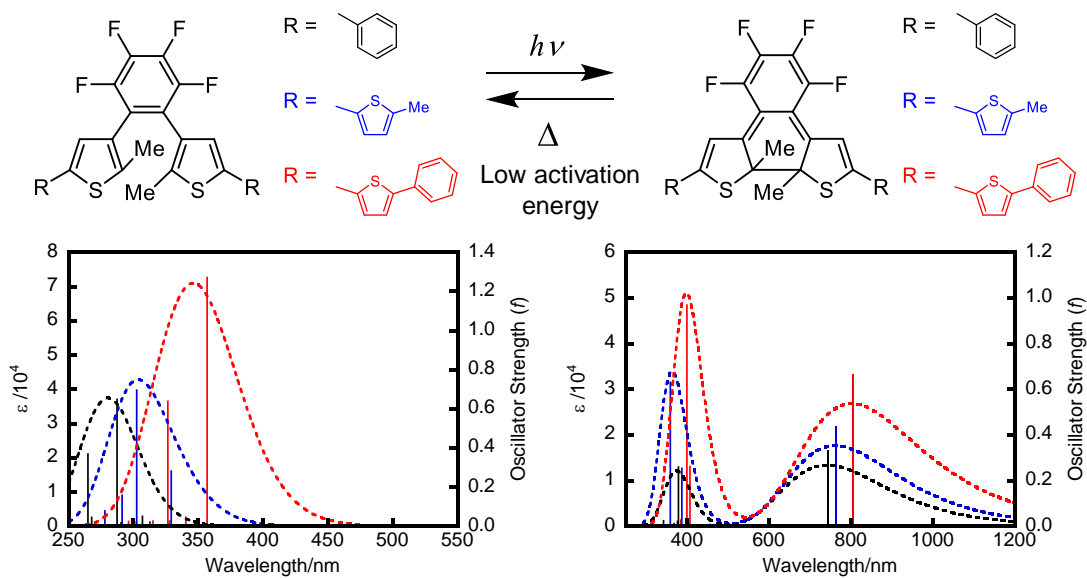
- diarylethenes having thermal functionality, *Chem. Rec.*, 2016, **16**, 2005-2015.
23. K. Inaba, R. Iwai, M. Morimoto and M. Irie, Thermally reversible photochromism of dipyrrolylethenes, *Photochem. Photobiol. Sci.*, 2019, **18**, 2136-2141.
 24. Y. Sato, D. Kitagawa and S. Kobatake, Molecular design for a write-by-light/erase-by-heat recording system using photochromic diarylethenes with thermal cycloreversion, *Tetrahedron*, 2019, **75**, 130487.
 25. D. Kitagawa, T. Nakahama, Y. Nakai and S. Kobatake, 1,2-Diarylbenzene as fast T-type photochromic switch, *J. Mater. Chem. C*, 2019, **7**, 2865-2870.
 26. T. Nakahama, D. Kitagawa and S. Kobatake, Tuning of optical properties and thermal cycloreversion reactivity of photochromic diarylbenzene by introducing electron-donating substituents, *J. Phys. Chem. C*, 2019, **123**, 31212-31218.
 27. M. J. Frisch, G. W. Trucks, H. B. Schlegel, G. E. Scuseria, M. A. Robb, J. R. Cheeseman, G. Scalmani, V. Barone, B. Mennucci, G. A. Petersson, H. Nakatsuji, M. Caricato, X. Li, H. P. Hratchian, A. F. Izmaylov, J. Bloino, G. Zheng, J. L. Sonnenberg, M. Hada, M. Ehara, K. Toyota, R. Fukuda, J. Hasegawa, M. Ishida, T. Nakajima, Y. Honda, O. Kitao, H. Nakai, T. Vreven, J. A. Montgomery, Jr., J. E. Peralta, F. Ogliaro, M. Bearpark, J. J. Heyd, E. Brothers, K. N. Kudin, V. N. Staroverov, R. Kobayashi, J. Normand, K. Raghavachari, A. Rendell, J. C. Burant, S. S. Iyengar, J. Tomasi, M. Cossi, N. Rega, J. M. Millam, M. Klene, J. E. Knox, J. B. Cross, V. Bakken, C. Adamo, J. Jaramillo, R. Gomperts, R. E. Stratmann, O. Yazyev, A. J. Austin, R. Cammi, C. Pomelli, J. W. Ochterski, R. L. Martin, K. Morokuma, V. G. Zakrzewski, G. A. Voth, P. Salvador, J. J. Dannenberg, S. Dapprich, A. D. Daniels, Ö. Farkas, J. B. Foresman, J. V. Ortiz, J. Cioslowski, and D. J. Fox, Gaussian 09 (Gaussian, Inc., Wallingford CT, 2009).

28. A. D. Becke, Density-functional thermochemistry. III. The role of exact exchange, *J. Chem. Phys.*, 1993, **98**, 5648-5652.
29. C. Lee, W. Yang and R. G. Parr, Development of the Colle-Salvetti correlation-energy formula into a functional of the electron density, *Phys. Rev. B: Condens. Matter*, 1988, **37**, 785-789.
30. J. P. Perdew and Y. Wang, Accurate and simple analytic representation of the electron-gas correlation energy, *Phys. Rev. B: Condens. Matter*, 1992, **45**, 13244-13249.
31. A. D. Boese and J. M. Martin, Development of density functionals for thermochemical kinetics, *J. Chem. Phys.*, 2004, **121**, 3405-3416.
32. Y. Zhao, N. E. Schultz and D. G. Truhlar, Exchange-correlation functional with broad accuracy for metallic and nonmetallic compounds, kinetics, and noncovalent interactions, *J. Chem. Phys.*, 2005, **123**, 161103.
33. Y. Zhao, N. E. Schultz and D. G. Truhlar, Design of density functionals by combining the method of constraint satisfaction with parametrization for thermochemistry, thermochemical kinetics, and noncovalent interactions, *J. Chem. Theory Comput.*, 2006, **2**, 364-382.
34. Y. Zhao and D. G. Truhlar, The M06 suite of density functionals for main group thermochemistry, thermochemical kinetics, noncovalent interactions, excited states, and transition elements: two new functionals and systematic testing of four M06-class functionals and 12 other functionals, *Theor. Chem. Acc.*, 2008, **120**, 215-241.
35. J.-D. Chai and M. Head-Gordon, Long-range corrected hybrid density functionals with damped atom-atom dispersion corrections, *Phys. Chem. Chem. Phys.*, 2008, **10**, 6615-6620.
36. R. Ditchfield, W. J. Hehre and J. A. Pople, Self-consistent molecular-orbital methods. IX.

- An extended gaussian-type basis for molecular-orbital studies of organic molecules, *J. Chem. Phys.*, 1971, **54**, 724-728.
37. T. Yanai, D. P. Tew and N. C. Handy, A new hybrid exchange-correlation functional using the Coulomb-attenuating method (CAM-B3LYP), *Chem. Phys. Lett.*, 2004, **393**, 51-57.
38. C. Adamo and V. Barone, Exchange functionals with improved long-range behavior and adiabatic connection methods without adjustable parameters: The mPW and mPW1PW models, *J. Chem. Phys.*, 1998, **108**, 664-675.
39. N. Brimhall, T. L. Andrew, R. V. Manthena and R. Menon, Breaking the far-field diffraction limit in optical nanopatterning via repeated photochemical and electrochemical transitions in photochromic molecules, *Phys. Rev. Lett.*, 2011, **107**, 205501.
40. S. Kobatake and M. Irie, Synthesis and photochromism of diarylethenes with isopropyl groups at the reactive carbons and long and π -conjugated heteroaryl groups, *Chem. Lett.*, 2003, **32**, 1078-1079.
41. P. D. Patel and A. E. Masunov, Theoretical study of photochromic compounds: Part 3. Prediction of thermal stability, *J. Phys. Chem. C*, 2011, **115**, 10292-10297.
42. X. Li, Q. Zou and H. Ågren, Photochromic diarylethenes with heterocyclic aromatic rings: Correlation between thermal bistability and geometrical characters of transition states, *J. Phys. Chem. A*, 2015, **119**, 9140-9147.
43. P. D. Patel and A. E. Masunov, Theoretical study of photochromic compounds. 1. Bond length alternation and absorption spectra for the open and closed forms of 29 diarylethene derivatives, *J. Phys. Chem. A*, 2009, **113**, 8409-8414.
44. R. Li, H. Arai, Y. Kobayashi, K. Mutoh and J. Abe, Molecular design to increase the photosensitivity of photochromic phenoxyl-imidazolyl radical complexes, *Mater. Chem.*

- Front.*, 2019, **3**, 2380-2387.
45. G. Pariani, M. Quintavalla, L. Colella, L. Oggioni, R. Castagna, F. Ortica, C. Bertarelli and A. Bianco, New insight into the fatigue resistance of photochromic 1,2-diarylethenes, *J. Phys. Chem. C*, 2017, **121**, 23592-23598.
46. A. Perrier, F. Maurel and D. Jacquemin, Interplay between electronic and steric effects in multiphotochromic diarylethenes, *J. Phys. Chem. C*, 2011, **115**, 9193-9203.

TOC



The best functional to predict the optical and thermal properties of DABs in DFT calculation was elucidated.